Photothermal dynamics of micro-glass beads coated with gold nanoparticles in water: fine bubble generation and fluid-induced laser trapping

Shin-ichiro Yanagiya, Naoya Sekimoto, and Akihiro Furube

[1]*Institute of Science and Technology, Tokushima University, 2-1 Minamijosanjima-cho, Tokushima, 770-8506, Japan*

Abstracts

In this study, gold nanoparticles were heterogeneously deposited onto the surface of glass beads through a gold ion reduction method to obtain "plasmonic beads." The plasmonic beads in pure water were illuminated with a visible continuous-wave laser through an objective lens. Using relatively lower-powered laser, the plasmonic beads were optically trapped and aggregated the other beads over an area much greater than the focal point. On the other hand, using a high-powered laser (> 20 mW/μm^2) produced microbubbles in water. Thus, the plasmonic beads studied herein can act as optically controllable fluid and microbubble generators.

[a)] Electronic mail: syanagiya@tokushima-u.ac.jp.

Introduction

In recent decades, gold nanoparticles (AuNPs) have attracted much attention in the field of nanoscience because of their special optical properties. AuNPs absorb specific wavelengths of light through an optical phenomenon known as localized surface plasmon resonance (LSPR). This phenomenon can be tuned from visible to infrared wavelengths depending on the shape and size of the AuNPs.[1–3] The LSPR enhances the Raman signals of biomolecules, known as surface-enhanced Raman scattering (SERS), and the use of SERS is ubiquitous for sensing applications.[4,5]

According to time-resolved spectroscopy, the light absorbed by AuNP is transformed into localized heat in nanoseconds.[6,7] The temperature can reach several hundred Celsius, but the quantity of heat is very small because of the tiny volume.[8] The heat rapidly transfers to a neighboring medium, and the AuNP temperature immediately returns to room temperature. If the temperature of the medium becomes higher than the critical temperature, a phase transition occurs. The phase transition of water results in a plasmonic boiling bubble.[9–13] A phase transition event occurring in biological cells can be used for photothermal therapy.[9,14,15]

A heated nanoparticle produces a high temperature gradient, and this results in convection heat flow. Donner et al. reported on strong hydrodynamic convection heat flow through FEM simulation investigations.[16] Namura et al. reported that the Marangoni effect was responsible for producing the strong convection flow.[17] If the heat source is fixed, the fluid would affect the particles and molecules in a solution. On the other hand, it is interesting question how a freely moving nano heat source affects particles and molecules in a solution.

AuNPs have been utilized in dispersed liquids[18,19] and by deposition or micro-patterning on a substrate.[20,21] Recently, AuNPs have been deposited in micro-spaces to observe the position of AuNPs optically and for easy AuNP handling. Reinher et al. demonstrated the use of optical fibers with heated

biological tissues.[15] Zhang et al. reported the use of plasmonic beads to detect biological macromolecules by SERS. [22]

In this study, AuNPs were deposited on micro-glass beads for use as plasmonic nano-heaters. The plasmonic beads were illuminated with a visible continuous-wave (CW) laser and observed using an inverted optical microscope in order to investigate the photothermal bubble dynamics, plasmonic convection flow around the bead, and optical manipulations.

Materials and methods

Plasmonic beads were fabricated according to the method reported by Zhang et al. The micro-glass beads (3–10 and 10–30 μm diameters) were purchased from Polysciences Inc. and washed with pure water before silane coupling treatment. The silane coupling agent was 3-(2-aminoethylamino)-propyltrimethoxysilane (AEPTS, Tokyo Chemical Industry Co., Ltd.). The beads were processed in an ethanol solution containing AEPTS for 18 h. The dispersion medium was changed to a $HAuCl_4$ solution, followed by gold ion reduction to form the AuNPs (20 min with magnetic stirring). Thereafter, the supernatant was replaced with pure water, and the beads were allowed to rest at room temperature. Some of the synthesized beads were dropped on a glass plate and treated thermally at 300 °C for 3 h in an electric oven. Surface morphology and elemental characterization were explored by scanning electron microscopy (SEM) and energy dispersive X-ray spectroscopy (EDS).

The photothermal effects of the beads were observed in situ using an inverted optical microscope (IX-71, Olympus Co.). The pure water-dispersed beads were sandwiched between two glass plates with a 1 mm spacer and placed on the microscope stage. A 473 nm CW laser was introduced from the back-port of the microscope and focused on the sample through an objective lens (LUCPlanSAPO 40× numerical aperture (NA) 0.6 or UPlanSAPO 10× NA 0.4, Olympus Co.) to illuminate the bead from the bottom at a laser power of 1–30 mW. The beam spot size for LUCPlanSAPO 40× on a flat glass plate was estimated

to be 1 μm^2, and thus the laser power density was about 1–30 mW/μm^2. And the laser power density for objective lens of 10x can be calculated from the numerical aperture ratio[23], that is;

$$\frac{\mathrm{I_{10x}}}{\mathrm{I_{40x}}} = \frac{\frac{P}{A_{10x}}}{\frac{P}{A_{40x}}} = \frac{w_{40x}^2}{w_{10x}^2} = \left(\frac{NA_{10x}}{NA_{40x}}\right)^2 = \frac{4}{9}$$

where I_i, P, A_i, w_i, and NA_i represent the laser power density, the total laser power, the spot area, the minimum beam waist, and the NA for the objective lenses of i=10x and 40x, respectively. Thus, the laser power density for the objective lens of UPlanSAPO 10x was lower than 13.3 mW/μm^2. The illuminated beads were monitored using a CCD camera at 1–10 frames/s. The convection flow was optically observed by exchanging pure water for a diluted colloidal suspension (100-nm silica (Fig. 4) or 2-μm polystyrene (PS, Fig. 5)).

Results and discussion

First, we examined the surface morphology and composition of the synthesized beads. Figure 1 shows the SEM images of the AuNPs on a glass bead post-thermal treatment. As shown in Figs. 1(a)-1(b), the gold nanoparticles, which was analyzed by EDS (Supporting Information 1), were homogeneously distributed. AuNPs are supposed to have successfully deposited on the glass beads. Figure 1(c) shows the AuNP diameter distribution in the range of 10 to 50 nm (average 20 nm) with a number density of 6×10^2 units/μm^2. From the viewpoint of photothermal effects, the size of AuNP affects not only an optical absorbance by LSPR but also a heat quantity. Larger AuNPs have higher calorific value at the same temperature and produce nanobubbles even at lower-powered laser.[12] When the laser power become higher, the neighbor nanobubbles unite and grow up to be a microbubble. Thus, it is important to control the size and density of AuNPS.

The dynamics of the plasmonic beads under CW laser illumination were observed using the optical microscope. We first demonstrated optical manipulation using a relatively low-powered CW laser (about 3 mW/μm^2) with irradiation from the objective lens of the lower NA (LUCPlanSAPO 10×, NA 0.4). Figures 2(a)-2(c) (movies available in Supporting Information 2) show snapshots of plasmonic bead migration caused by CW laser trapping while moving the microscope stage. When the laser was switched on and one glass bead was illuminated, the neighboring beads aggregated immediately. Then, the aggregated beads kept their position around the focus, even while the stage was moved. This aggregation outside of a focus area phenomenon has also been reported for colloidal particles by Kudo and Wang et al.[24,25] Against previous works, the plasmonic bead was two orders of magnitude bigger, and the affected area was larger.

General optical manipulations arose from the electric field gradient, in other words, the dielectric object in the Gaussian beam laser.[26] Therefore, this phenomenon was not supposed to be similar to optical tweezers. The phenomenon was believed to be an attraction of other beads to the trapped bead. To observe optical gathering more, a greater number of beads were illuminated using a higher power laser. Figures 2(d)-2(f) (Supporting Information 3) show snapshots of the gathering and moving of plasmonic beads at about 8 mW/μm^2. About 50 particles immediately aggregated when the laser was switched on. The beads gathered from distances greater than several tens of μm, and the aggregate remained trapped within the focus area even while the stage was moved. Note that some beads external to the bead aggregate maintained their distance of approximately 100 μm away from the laser spots in a concentric pattern as shown in Fig. 2(f).

When the plasmonic beads were trapped and manipulated by the CW laser, no bubble was observed with the optical microscope. Next, we demonstrated visible microbubble generation by the laser irradiation of higher power density using a higher-powered objective lens (LUCPlanSAPO 40×, NA 0.6). Figure 3

shows snapshots of the emergence of microbubbles from 30 mW CW laser irradiation. The microbubbles were generated when the laser was focused on the surface of the plasmonic bead. It was difficult to determine the laser power density criteria because the focal plane and the irradiated area of the CW laser varied with the exact bead site. However, we could observe microbubble generation even at 20 mW. Thus, we empirically defined the possible laser power density of bubble generation as 20 mW/μm^2.

The generated microbubble can be distinguished by two processes: bead surface attachment and dissociation from the bead surface with successive microbubble generations. Figures 3(a) and 3(b) (Supporting Information 4) show the optical images of the bubble growth. The CW laser illumination immediately generated one bubble at the focus. The microbubble adhered to the surface of the bead. The silane-coated surface was relatively hydrophobic and might act as a bubble-linker. To test the hypothesis, the beads were heated at 300 °C for 3 h in an electric furnace to remove the silane residue (see Supporting Information 1). The beads gently fixed on the substrate when they were heated. Then the beads stopped their motion even under the laser irradiation. Under the condition, we could observe the microbubble motion without interruption by other beads' motion. The snapshots of the dynamics of generated microbubbles and the schematic side view are shown in Figs. 3(d), 3(e), and 3(f) (Supporting Information 5). The microbubbles on the silane-free bead had larger contact angle compared to as-synthesized surface. In addition, the microbubble detached from the sample and moved upward and aggregated again. We supposed that the hydrophobicity of the bead surface can control the microbubble behavior.

Plasmonic bubbles were studied under various generation conditions. Freely dispersed AuNPs in solution were heated by laser pulses, and plasmonic nanobubbles that lived for nanoseconds were generated.[7,13,27)] Microbubbles that grew from nanobubbles incorporation were observed on the AuNP covered glass plate.[6,8)] By the same principle, the microbubbles in this study were generated from direct laser illumination of AuNP on the bead surface. On the other hand, microbubbles were occasionally

observed on the top-most surface of the glass bead. In that case, the micro-bead acted as a ball lens and changed the focal point.[28] The focal point gap can be eliminated by setting the refractive index of the solution to that of the glass bead. Alternatively, the focal point can be fixed by embedding the bead into a photonic device, like an optical fiber.

To investigate the convection flow around the microbubble and the bead, we observed the laser-induced microbubble in a diluted colloidal suspension of colloidal silica. Figures 4(a)-4(d) show the optical images of the convection induced by the CW laser irradiation (Supporting Information 6). When the bubble generated, the convection flow was clearly observed a few second after the bubble generation as shown in Figs. 4(a) and 4(b). The bright contrast arose from the scattering light of silica colloids that aggregated during the flow. The schematic model of the flow is depicted in Fig. 4(e). The main flow seemed to start along the bubble surface as indicated by A in Fig. 4(b) and 4(c), and circulated near the surface. Namura et al reported the Marangoni effect of the bubble generated by laser irradiation of gold thin film is the driving force of the flow.[29] In our system, the flow along the bubble was constantly observed and also arose from the Marangoni effect as indicated by red arrow in Fig. 4(e). On the other hand, the circulating flow occasionally changed its path as shown in Fig. 4(b) and 4(c). The flow path was turbulence and depended not only on the illuminated bead but also neighbor beads and an aqueous solution. The satellite beads in Fig. 2(f) should be caused by a localized vortex flow, however, it needs three-dimensional study to become clear how and why the flow generated.

Next, we also investigated the convection flow during the laser trapping, which was observed in Fig. 2. Figure 5 shows the optical images of a laser trapped plasmonic bead in diluted PS colloidal suspension (Supporting Information 7). When the bead approached the focus of CW laser (wavelength; 532 nm, objective lens; x10, laser power density; 6.7 $mW/\mu m^2$), the convection flow immediately generated even no microbubble generated. The PS particles circulated around the bead on the glass plate. The circulation

flow was very fast and larger than 500 μm in diameter. As shown in Figs. 5(b)-5(d), a free bead was caught in the current and stayed near the trapped bead.

Our results indicated that the CW laser illumination of plasmonic beads produced not only thermal phenomena such as bubble generation, but also fluid phenomena such as laser manipulation and laser aggregation. We next investigated the FEM simulation of the 2D hydrodynamics around the beads using the COMSOL program. In previous studies, optifluid[16] and Marangoni effects[30] of the heated AuNPs were investigated on a glass plate. We started from these models and changed the substrate from a flat plate to a spherical object.

Figure 6a depicts the model of a part of the system around the heated AuNP. To simplify the model, only one AuNP (30 nm in diameter) was placed on the top of a glass bead. The AuNP temperature was kept at 600 K, which is near the spinodal temperature of water (550 K)[31,32]. Figure 6(b) shows the temperature distribution around the AuNP. Temperature regions higher than 100 °C existed within a 200 nm square, and we set the air bubble of ϕ200 nm to cover the region entirely. As shown in Fig. 6(c), the temperature gradient along the bubble was on the order of 10^8 K/m, which is the driving force of Marangoni convection. The value was supposed to be sufficiently large to be the source of a convection flow. To investigate the interaction between neighboring glass beads, two glass beads of the same size were placed on a glass plate at a distance of 1.5 μm, as shown in Figures 6d and 6e, and surrounded by water. The water area was 3 × 6 μm, and the thickness of the glass plate was 500 nm. The water was expected to display incompressible flow and obey the Navier–Stokes equation:

$$\rho(\boldsymbol{u}\cdot\nabla\boldsymbol{u}) = -\nabla p + \nabla\cdot\left(\mu(\nabla\boldsymbol{u} + (\nabla\boldsymbol{u})^T)\right) + \boldsymbol{F},$$

where $\boldsymbol{u}$, μ, and p are the fluid velocity, dynamic viscosity, and pressure, respectively. The Marangoni flow along the bubble–water interface was also considered. Marangoni flow was used in an additional heat transfer module and was calculated according to the following equation:

$$[\mu(\nabla \boldsymbol{u} + (\nabla \boldsymbol{u})^T)] \cdot \mathbf{n} = \gamma \nabla_t T$$

$$\gamma = \left|\frac{\partial \sigma}{\partial T}\right|,$$

where σ is the surface tension and γ is the surface tension temperature dependence.

Figures 6(d) and 6(e) show the pressure distribution of water with and without the bubble. As shown in Fig. 6(d), the region between the beads had a lower pressure than the outer region by approximately 10^5 Pa. On the other hand, the pressure difference of the system without the bubble was very small (~10^{-1} Pa) as shown in Fig. 6(e). This indicated that the bubble and accompanying Marangoni effects played important roles in our laser trapping results. The flow direction is shown in Fig. 6(f). The Marangoni flow maximized at the maximum temperature gradient along the bubble–water interface, and the direction of the flow was upward. Because the side beads were immobile, the flow from the side was interrupted, and the density between the beads was low. If the beads could move freely, they should have aggregated with the heated bead, which would agree with the laser trapping experiment (Fig. 2).

A FEM simulation study suggests that, as above stated, only nanobubble of 200 nm in diameter produced hundreds of times larger convection flow through a Marangoni effect. In addition, when we manipulated the beads, the plasmonic bead sparkled during the laser irradiation. We supposed that this was the scattering light of the plasmonic nanobubble. We concluded that the achievements in our study was due to the plasmonic nano- and micro-bubbles generated from photothermally heated AuNPs.

Conclusion

We fabricated plasmonic beads on which AuNPs were heterogeneously deposited through the $NaBH_4$ reduction method. The plasmonic beads were optically manipulated and generated bubbles when irradiated with visible CW laser light. Optical trapping and bead aggregation could be achieved at laser powers greater than 3 mW/μm^2. A higher laser power leads to increased bead aggregation. When the laser power density was larger than 20 mW/μm^2, the bubble was generated on the surface of the plasmonic bead. Microbubble growth could be divided into two categories: adhesion to the surface and immediate release from the surface depending on whether the beads were thermally treated to remove the silane coating. The observation of the convection flow and FEM simulation study suggested that the Marangoni effects induced by temperature differences at the surface of a small bubble acted as the driving force for optical confinement and optical attraction. These results suggest that plasmonic beads have potential applications as optically controllable nano-heaters, nano-bubble generators, and micro-convection generators.

Acknowledgement

This work was supported by the Japan Society for the Promotion of Science (JSPS) KAKENHI (Grant No. 15K04679). The authors also thank Satoshi Sugano for his EDS analysis of plasmonic beads. The authors would like to thank Enago (www.enago.jp) for the English language review.

References

1) H. Chen, L. Shao, Q. Li, J. Wang, Chem. Soc. Rev. **42**, 2679 (2013).
2) X. Ye, C. Zheng, J. Chen, Y. Gao, C.B. Murray, Nano Lett. **13**, 765 (2013).
3) C. Fang, G. Zhao, Y. Xiao, J. Zhao, Z. Zhang, B. Geng, Sci. Rep. **6**, 1 (2016).
4) D.M. Chevrier, A. Chatt, P. Zhang, J. Nanophotonics **6**, 64504 (2012).
5) L. Vigderman, B.P. Khanal, E.R. Zubarev, Adv. Mater. **24**, 4811 (2012).
6) M.L. Brongersma, N.J. Halas, P. Nordlander, Nat. Nanotechnol. **10**, 25 (2015).
7) T. Katayama, K. Setoura, D. Werner, H. Miyasaka, S. Hashimoto, Langmuir **30**, 9504 (2014).
8) K. Setoura, D. Werner, S. Hashimoto, J. Phys. Chem. C **116**, 15458 (2012).
9) V.P. Zharov, K.E. Mercer, E.N. Galitovskaya, M.S. Smeltzer, Biophys. J. **90**, 619 (2006).
10) Z. Fang, Y.R. Zhen, O. Neumann, A. Polman, F.J. García De Abajo, P. Nordlander, N.J. Halas, Nano Lett. **13**, 1736 (2013).
11) T. Nakajima, X. Wang, S. Chatterjee, T. Sakka, Sci. Rep. **6**, 1 (2016).
12) E. Lukianova-Hleb, Y. Hu, L. Latterini, L. Tarpani, S. Lee, R.A. Drezek, J.H. Hafner, D.O. Lapotko, ACS Nano **4**, 2109 (2010).

13) J. Lombard, T. Biben, S. Merabia, J. Phys. Chem. C **121**, 15402 (2017).
14) L.R. Hirsch, R.J. Stafford, J.A. Bankson, S.R. Sershen, B. Rivera, R.E. Price, J.D. Hazle, N.J. Halas, J.L. West, Proc. Natl. Acad. Sci. **100**, 13549 (2003).
15) R. Pimentel-Domínguez, P. Moreno-Álvarez, M. Hautefeuille, A. Chavarría, J. Hernández-Cordero, Biomed. Opt. Express **7**, 1138 (2016).
16) J.S. Donner, G. Baffou, D. McCloskey, R. Quidant, ACS Nano **5**, 5457 (2011).
17) K. Namura, K. Nakajima, M. Suzuki, Nanotechnology **29**, 065201 (2018).
18) D. Lapotko, Cancers (Basel). **3**, 802 (2011).
19) O.A. Yeshchenko, N. V. Kutsevol, A.P. Naumenko, Plasmonics **11**, 345 (2016).
20) T.U. Tumkur, X. Yang, B. Cerjan, N.J. Halas, P. Nordlander, I. Thomann, Nano Lett. **16**, 7942 (2016).
21) D.A. Boyd, L. Greengard, M. Brongersma, M.Y. El-Naggar, D.G. Goodwin, Nano Lett. **6**, 2592 (2006).
22) B. Zhang, J. Yang, Y. Zou, M. Gong, H. Chen, G. Hong, A.L. Antaris, X. Li, C.-L. Liu, C. Chen, H. Dai, Chem. Sci. **5**, 4070 (2014).
23) A. Yariv, P. Yeh, A. Yariv, Photonics : Optical Electronics in Modern Communications, n.d.
24) T. Kudo, S.F. Wang, K.I. Yuyama, H. Masuhara, Nano Lett. **16**, 3058 (2016).
25) S.F. Wang, T. Kudo, K.I. Yuyama, T. Sugiyama, H. Masuhara, Langmuir **32**, 12488 (2016).
26) M. Dienerowitz, J. Nanophotonics **2**, 021875 (2008).
27) A. Siems, S.A.L. Weber, J. Boneberg, A. Plech, New J. Phys. **13**, (2011).
28) M.J. Riedl, Society of Photo-optical Instrumentation Engineers., Optical Design Fundamentals for Infrared Systems, SPIE, 2001.
29) K. Namura, K. Nakajima, K. Kimura, M. Suzuki, J. Nanophotonics **10**, 033006 (2016).
30) K. Namura, K. Nakajima, M. Suzuki, Sci. Rep. **7**, 1 (2017).
31) J. Lombard, T. Biben, S. Merabia, Phys. Rev. E **91**, 043007 (2015).
32) K. Metwally, S. Mensah, G. Baffou, J. Phys. Chem. C **119**, 28586 (2015).

Figure captions

FIG. 1. (a) SEM image of a micro-glass bead covered with AuNPs whose composite characterization was confirmed by EDS. (b) Enlarged SEM image of AuNPs on the glass bead. (c) Size distribution of the AuNPs in the area of 500×500 nm^2 for ten beads.

FIG. 2. (color online) Snapshots of optical manipulation of the beads: (a-c) The motion of plasmonic beads using the CW laser. During the stage was moved down and right, the beads remained confined to the area around the laser spot. (d-f) More plasmonic beads aggregation by higher power laser. When a 30 mW CW laser illuminated a specific bead, the surrounding beads immediately aggregated and also remained trapped. While moving the aggregated beads, some external beads formed concentric pattern external to the bead aggregate. Their distance from laser spot was approximately 100 μm.

FIG. 3. (color online) Snapshots of microbubble generation on the plasmonic bead when the laser was focused on the surface. (a, b) Microbubbles generated at the laser spot remained on the surface. When the stage was moved, the bubble also moved with rotating the bead. (d, e) Bubbles generated at the laser spot and immediately separated from the bead surface. The bubble detached from the illuminated bead surface and united in the other place. (c, f) Schematic side views of the bead and the microbubbles.

FIG. 4. (color online) (a-d) Optical images of laser-induced convection flow around the bubble in a diluted colloidal suspension of silica. The lightness contrast that arose from the scattering light of aggregated silica colloids (d). The image contrast was enhanced using an image processing software. The spots of laser irradiation in (a-c) were represented by a x-mark. (e) Schematic model of the system. The red and the blue lines indicate the flow of the colloidal suspension.

FIG. 5. Optical images of laser-induced convection flow around the bubble in a diluted colloidal suspension of polystyrene (PS, 2 μm in diameter). (a) The laser irradiated the point illustrated by a cross with the laser power of 6.7 mW/μm^2 through x10 objective lens (NA=0.4). The bead approached the focal point by moving the stage as indicated by a gray arrow. (b) The convection flow, which was indicated by white arrow, immediately generated when the bead was irradiated. Another bead labeled by B in the figure was involved the convection and went along the flow as illustrated by white dashed arrow. (c) The PS particles circulated along with the flow illustrated by white arrows. (d) After switching off the laser, we could observe the PS particles gathering in a fan-like shape.

FIG. 6. (color online) FEM simulation of the water hydrodynamics around the plasmonic bead: (a) schematic model around a heated AuNP. Region A is the supplementary vapor space that was hotter than 100 °C. (b) Thermal distribution around the AuNP when the AuNP was 600 K. (c) Temperature profile along the bubble surface indicated by arrow ΔT in Fig. 6a. The origin of the distance indicates the contact point between the bubble and region A. Pressure distribution (d) with and (e) without the bubble. (f) The distribution of flow speed of the system under bubble-forming conditions.

FIGURES

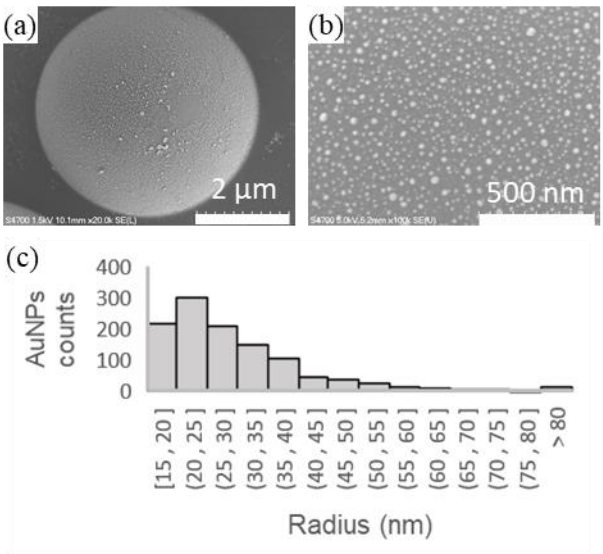

Figure 1

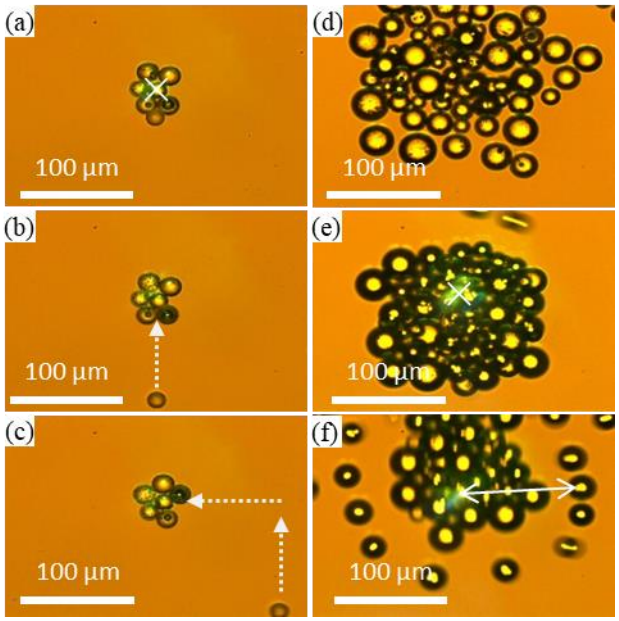

Figure 2

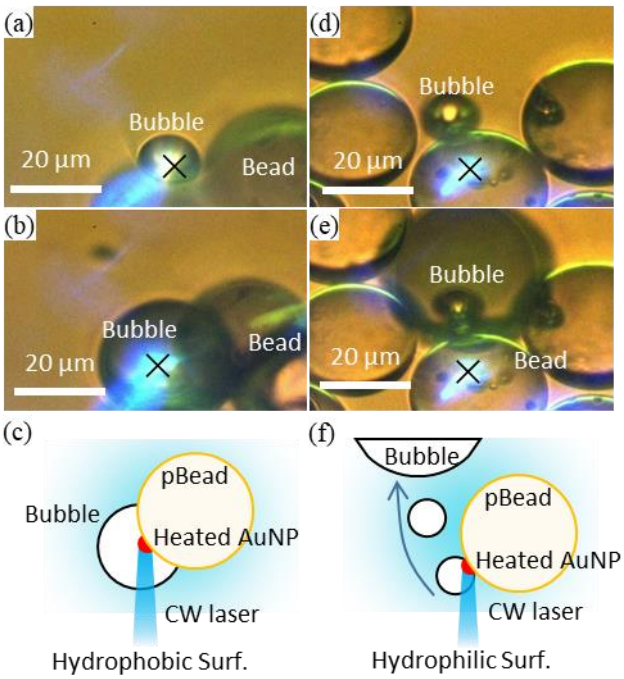
(a)
Bubble
20 µm
Bead
(d)
Bubble
20 µm
(b)
Bubble
20 µm
Bead
(e)
Bubble
20 µm
Bead
(c)
pBead
Bubble
Heated AuNP
CW laser
Hydrophobic Surf.
(f)
Bubble
pBead
Heated AuNP
CW laser
Hydrophilic Surf.

Figure 3

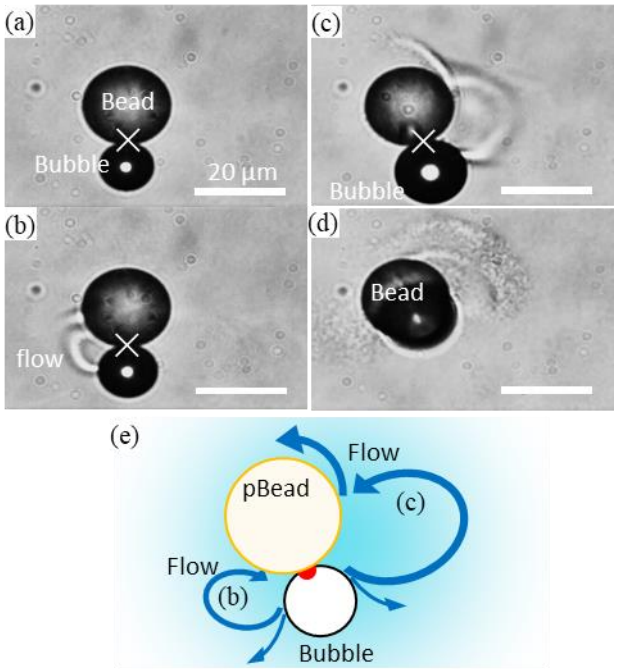
(a)
Bead
Bubble
20 µm
(c)
Bubble
(b)
flow
(d)
Bead
(e)
Flow
pBead
(c)
Flow
(b)
Bubble

Figure 4

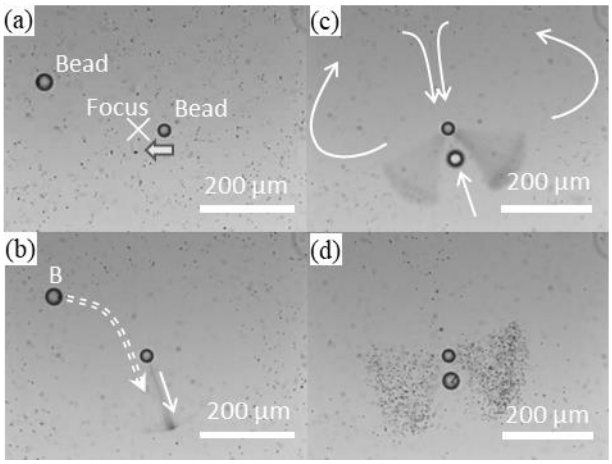

Figure 5

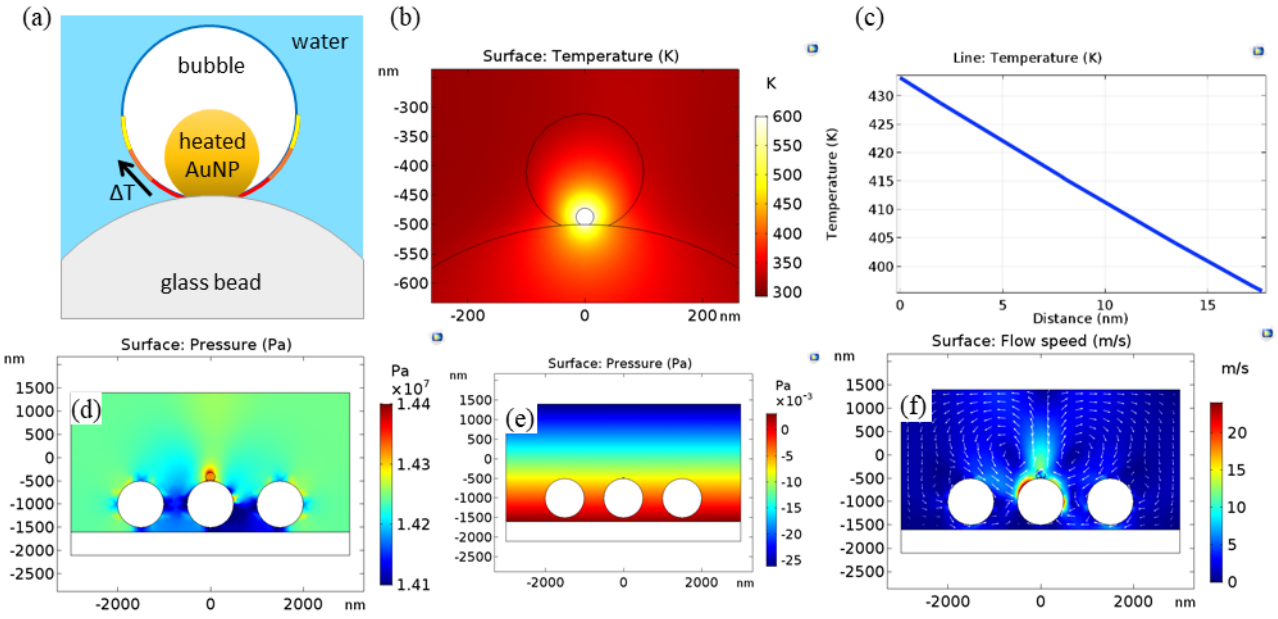
(a)
water
bubble
heated
AuNP
ΔT
glass bead
(b)
Surface: Temperature (K)
K
(c)
Line: Temperature (K)
Temperature (K)
Distance (nm)
Surface: Pressure (Pa)
(d)
Surface: Pressure (Pa)
(e)
Surface: Flow speed (m/s)
(f)
nm
m/s
Pa

Figure 6